WELDABILITY AND MECHANICAL PROPERTY OF $Ni_{53}Nb_{20}Ti_{10}Zr_8Co_6Cu_3$ METALLIC GLASS FOIL BY LASER WELDING

Takuya Tsumura, Katsunori Kobayashi*, Kazuhiro Nakata
Joining and Welding Research Institute, Osaka University
Ibaraki, Osaka 567-0047, Japan

Natsuki Yoneyama
Research Laboratory, Ishikawajima-Harima Heavy Industries Co. Ltd.
Isogo-ku, Yokohama, Kanagawa 235-8501, Japan

Taichi Murakami
Institute of Multidisciplinary Research for Advanced Materials, Tohoku University
Aoba-ku, Sendai, Miyagi 980-8579, Japan

Hisamichi Kimura, Akihisa Inoue
Institute for Materials Research, Tohoku University
Aoba-ku, Sendai, Miyagi 980-8577, Japan

ABSTRACT

In order to evaluate the weldability of a melt-spun Ni-based metallic glass foil with a thickness of 25 μm, bead-on-plate laser welding was carried out at different welding speeds from 2 to 12 m/min using a diode laser beam with a constant laser power of 26 W and wavelength of 808 nm. A sound weld bead, while maintaining the amorphous state, was successfully obtained at a high welding speed of 12 m/min; under these conditions, the weld bead consisted of an amorphous matrix with a very small amount of nanocrystals with a mean diameter of 14 nm. The hardness was almost the same as that of the base metal (740 HV), and the mean tensile strength of the weld bead was 1312 MPa, which is 56% of that of the base metal. At a lower welding speed of less than 6 m/min, a fusion zone appeared in the central zone of the weld bead consisting of the amorphous matrix with comparably large crystals with mean diameter of 170 nm. Further, the heat-affected zones adjacent to the fusion zone consisted of a completely crystallized structure with a high hardness of around 1200 HV, which caused a low joint strength or weld cracking due to the brittleness of crystallization or structural relaxation.

INTRODUCTION

Since the late 1980s, a number of amorphous alloys were found that exhibited a large supercooled liquid region through a distinct glass transition without any crystallization[1–3]; they were called bulk amorphous alloy, bulk glassy alloy, or metallic glass. The weldability of Zr-based metallic glass which is well known as a bulk metallic glass system with a large supercooled liquid region of about 100 K, has already been studied by spark welding[4], friction welding[5,6], and electron beam welding[7,8]. Ni-Nb-Ti-Zr-based bulk metallic glasses, which have been recently developed, have a high tensile strength, high corrosion resistance, and high crystallization temperature[9–11]. These Ni-based metallic glass alloys are expected to be applied as separator plates in solid polymer electrolyte fuel cells[11,12]. However, there has been no research conducted on the weldability of thin metallic glass sheet with a thickness lesser than 1 mm. If the welding of metallic glass with a thin sheet can be achieved by maintaining the amorphous phase, it can be expected to have wide applications in various industrial fields. The features of laser

welding are local heating, high cooling rate due to the high energy density, and the process is carried out in atmosphere. Therefore, it is expected to be an effective process for welding thin metallic glasses. In this study, the diode laser welding process was applied to a ribbon-shaped Ni-Nb-Ti-Zr-based metallic glass with a thickness of 25 μm, and the weldability was investigated as a first attempt at the laser welding of thin metallic glasses.

EXPERIMENTAL PROCEDURE

$Ni_{53}Nb_{20}Ti_{10}Zr_8Co_6Cu_3$ (nominal atomic %) metallic glass specimen was fabricated in a ribbon shape with a width of 50 mm and average thickness of 25 μm by melt spinning[9]. The thermal stability associated with the glass transition, supercooled liquid region, and crystallization was examined by differential scanning calorimetry at a heating rate of 0.67 K/s, and the melting temperature was measured by differential thermal analysis[9]. The glass transition temperature (T_g), crystallization temperature (T_x), and melting point (T_m) of this alloy are 846 K, 897 K, and 1265 K, respectively[9].

Figure 1 shows the schematic views of the setup and Table I shows the welding conditions. The bead-on-plate welding of the specimen was conducted using a diode laser unit (KLY-HP300α). The diode laser beam with a wavelength of 808 nm was delivered using a glass fiber with a diameter of 0.3 mm, and it was focused on the specimen surface with a spot diameter of 0.3 mm at an angle of 80°. The specimen was fixed on a copper backing plate with a groove of 2 mm width by a copper cover plate of 2 mm thickness with a slit of 2 mm width. Argon was used as a shielding gas with a flow rate of 10 *l*/min for the central shield and 5 *l*/min for the backing shield. The welding speed was varied from 2 to 12 m/min at a laser power of 26 W.

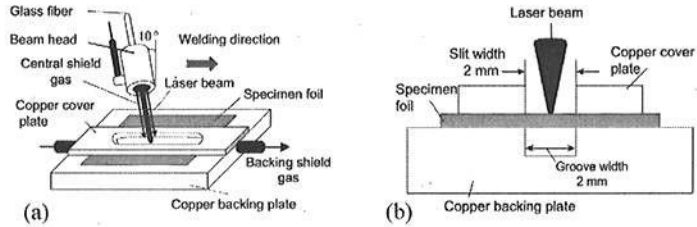

Figure 1 Schematic view of specimens during laser welding in the Ni-based metallic glass (a) setup of laser head and specimen holder and (b) cross-sectional view of specimen holder.

Table I Welding conditions used.

Welding type: Bead-on-plate	Welding speed: 2~12 m/min
Laser power: 26 W	Head angle: 10° advanced
Wavelength: 808 nm	Center shield gas: Ar, 10 l/min
Fiber diameter: 0.3 mm	Backing shield gas: Ar, 5 l/min
Spot diameter: 0.3 mm	Slit width: 2 mm
Focus: On the specimen surface	Groove width: 2mm

The surface of the welded specimen was examined using an optical microscope (OM) and by scanning electron microscopy (SEM). Micro-area X-ray diffraction (XRD) analysis, with a beam diameter of 50 μm (CuKα), tube voltage of 30 kV, and tube current of 50 mA was carried out at the center of the weld bead as well as the base metal to identify the amorphous phase. For the comparison of the XRD pattern of the crystallized phase, an annealed specimen that was

heated at 973 K for 60 min and cooled in a furnace for recrystallization was used. The cross section of the welded specimen was observed using an OM; further, the microhardness profile at the center of thickness was measured at intervals of 30 μm with 0.49 N for 15 s. Moreover, the microscale crystalline phase was minutely examined using a transmission electron microscope (TEM) with an acceleration voltage of 200 kV and magnification range of 50 000 to 100 000 for light field observations. The tensile specimen with a gauge section of 25 μm × 12.5 mm was cut out of the specimen before welding for the base metal and after welding for the welded specimen respectively, using a spark-erosion wire cutting machine. The tensile test was performed on the specimen at room temperature at a crosshead speed of 0.5 mm/min.

RESULT AND DISCUSSION

Figure 2 shows the bead appearance of the welded specimen by OM and SEM at welding speeds of 2, 4, 6, and 12 m/min. The width of the weld bead decreases with an increase in the welding speed, in other words with a lower heat input per unit length. The crack along the welding direction occurred in the weld bead at the welding speed of 2 m/min, and the transverse crack occurred in the weld bead at the welding speed of 4 m/min. However, at welding speeds above 6 m/min, the crack was not observed. It is thought that the residual stress under the cooling process as well as the existence of the brittle crystalline phase may possibly be the main causes of these cracks at welding speeds below 4 m/min.

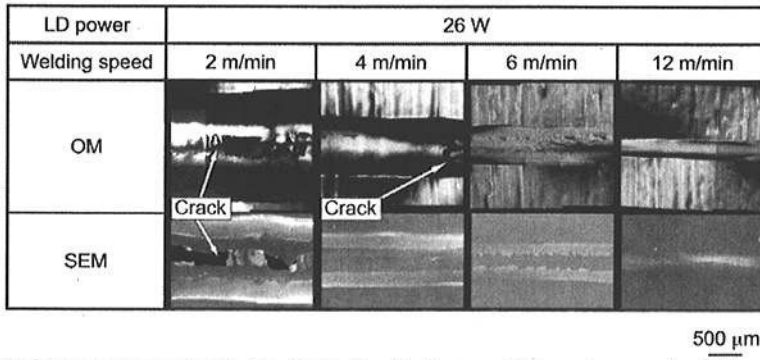

Figure 2 Bead appearance in $Ni_{53}Nb_{20}Ti_{10}Zr_8Co_6Cu_3$ laser welded specimens using OM and SEM at the welding speeds of 2, 4, 6, and 12 m/min with a constant laser power of 26 W.

Figure 3 shows the XRD patterns for the center of the weld bead surface with a constant laser power of 26 W in comparison with those for the base metal and the annealed specimen. The patterns of the base metal consist only of broad peaks showing the particular patterns obtained from the amorphous phase. On the other hand, diffraction peaks due to a crystalline phase are observed in the annealed specimen. In the weld bead, the patterns observed at the welding speeds below 4 m/min indicated the existence of the crystalline phase, but the pattern observed at welding speed of 12 m/min indicated the existence of the amorphous phase. At the welding speed of 6 m/min, the patterns seem to indicate the coexistence of the crystalline and amorphous phase. These results thus indicate that a sound weld bead could be obtained at a welding speed greater than 12 m/min while maintaining the amorphous state.

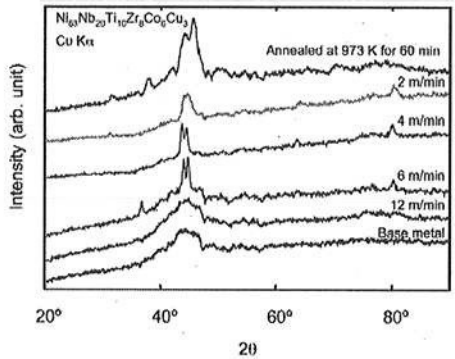

Figure 3 XRD patterns of $Ni_{53}Nb_{20}Ti_{10}Zr_8Co_6Cu_3$ laser welded specimens for the center of the weld bead at welding speeds of 2, 4, 6, and 12 m/min with a constant laser power of 26 W, base metal, and annealed specimen at 973 K for 60 min.

From the bead appearance determined by OM and SEM the welding speed of 6 m/min, as shown in Fig. 2, the weld bead consists of three zones, which are schematically shown in Fig. 4. These are zone I, with a rather jagged boundary at the weld bead center; zone II, with a smooth surface at both sides of zone I; and zone III, with a different surface state as compared to zone II and a very narrow strip that is adjacent to the base metal (B.M.). Zone I is the melted zone based on the presence of a ripple surface in it. Therefore, zones II and III are the heat-affected zones. Here, we denote zones II and III as HAZ-1 and HAZ-2, respectively. At the welding speed of 12 m/min, however, the weld bead did not melt because the ripple surface could not be observed, as shown in Fig. 2. Therefore, the weld bead may consist of HAZ-1 and/or HAZ-2

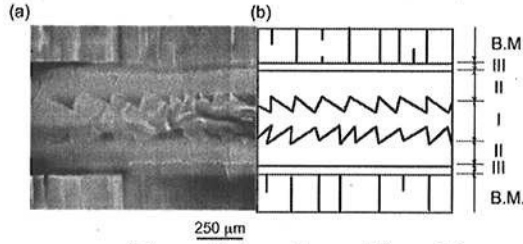

Figure 4 (a) Bead appearance of the welded specimen at the welding speed of 6 m/min, (b) schematic illustration of different zones in the weld bead.

The cross-sectional views of the microstructure and hardness profiles along with the center of the thickness at a welding speed of 6 m/min and 12 m/min are shown in Fig. 5. As shown in Fig. 5 (a), the hardness of the HAZ-2 zone was almost the same as that of the B.M. However, the hardness of the HAZ-1 zone in which the etch pit appeared, increased up to 1200 HV, and the hardness decreased to the same level as that of the base metal at the melted zone. Therefore, a close relationship is revealed between the weld structure and the hardness. On the contrary, as shown in Fig. 5 (b), the hardness is the same as that of the base metal and the etch pit cannot be seen in the weld bead for the welding speed of 12 m/min. Therefore, in this case, almost the entire welded bead consists of the HAZ-2 zone.

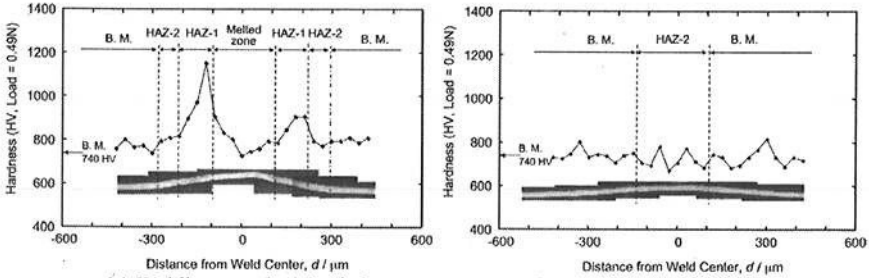

(a) Welding speed of 6 m/min (b) Welding speed of 12 m/min

Figure 5 Relation between microstructure and hardness profile on the welded specimen.

Figure 6 shows the TEM micrographs of the B.M. and the weld bead at the welding speed of 6 m/min and 12 m/min. As shown in Figs. 6 (a2) and (b2), the B.M. is a typical uniform amorphous structure and harrow ring is observed by selected-area electron diffraction. As shown in Fig. 6 (a4), the crystals with a mean diameter of 170 nm exist in the amorphous matrix as well as in the diffraction pattern for the combination of the harrow ring with the diffraction pattern by crystal at the melted zone. In slight contrast, as shown in Fig. 6 (a3), the HAZ-1 zone crystallized completely with a mean diameter of 400 nm into a clearer diffraction pattern than that of the melted zone. On the other hand, the weld bead consists of the amorphous matrix with a very small amount of nanocrystals with a mean diameter of 14 nm at the welding speed of 12 m/min, as shown in Fig. 6 (b3); this is quite different from the HAZ-1 zone images shown in Fig. 6 (a3).

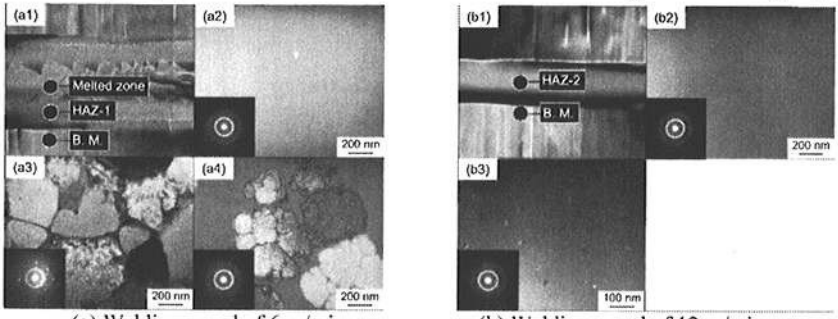

(a) Welding speed of 6 m/min (b) Welding speed of 12 m/min

Figure 6 TEM observed positions and micrographs of the weld bead: (a1) observed position at the welding speed of 6 m/min, TEM micrographs (a2) in B.M., (a3) in HAZ-1, (a4) in melted zone; and (b1) observed position at the welding speed of 12 m/min, TEM micrographs (b2) in B.M., (b3) in HAZ-2.

It was reported that the heat-affected zone crystallized more easily than the melted zone because the nose time of the TTT diagram of the metallic glass was much smaller than that of the melt[4]. In this study, the same results were concluded from the comparison of the degree of crystallization of the melted zone with that of HAZ-1, as shown in Figs. 5 (a), 6 (a3), and 6 (a4). Therefore, as shown in Fig. 4 (b), the weld bead shows three different zones (melted zone, HAZ-1, and HAZ-2) due to this feature.

Figure 7 shows the tensile strength of the base metal (B.M.) and the welded specimen at the welding speeds of 6 m/min and 12 m/min. The bars in Fig. 9 indicate the average strength. In the B.M. specimen, several fracture positions were observed. However, the fracture positions of the welded specimen were mainly in the weld metal. As an explanation for the varied strengths, it is theorized that the specimen edge by spark-erosion wire cutting is markedly uneven and/or the thickness of the specimen along its width is non-uniform. The average strength of the B.M. was 2334 MPa. Since the welded specimen at the welding speed of 6 m/min exhibits a crystalline structure, the average strength decreased to 771 MPa, which was about 32% of that of the B.M. The average strength of the specimen at the welding speed of 12 m/min was 1312 MPa, which was about 56% of that of the B.M. despite the absence of the crystalline structure. The reduction in the strength could be attributed to the concentration of stress at wrinkled surfaces, cracks starting from the nanocrystals in the weld bead, and the structural relaxation[1] caused by thermal history.

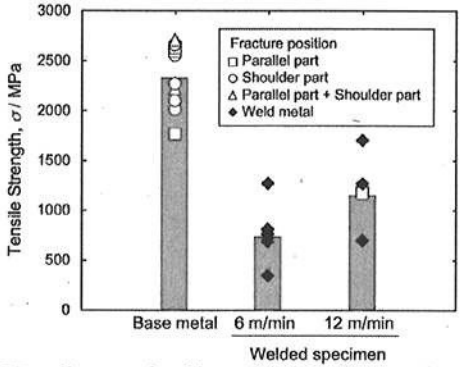

Figure 7 Tensile strength of the welded specimen and base metal.

CONCLUSIONS

The bead-on-plate welding of a melt-spun specimen of $Ni_{53}Nb_{20}Ti_{10}Zr_8Co_6Cu_3$ metallic glass was performed and the resulting microstructure of the laser weld bead and its mechanical properties were investigated. The following conclusive remarks were derived from this study.

(1) A sound weld bead can be obtained by diode laser welding at the welding speeds of 6 m/min and 12 m/min with a laser power of 26 W. The XRD pattern at the welding speed of 12 m/min exhibited the maintenance of the amorphous phase.

(2) At welding speeds lower than 6 m/min, the fusion zone of the weld bead consisted of the amorphous matrix with comparatively large crystals with a mean diameter of 170 nm, and the HAZ-1 consisted of a completely crystallized structure with a high hardness of around 1200 HV. At the welding speed of 12 m/min, the weld bead consisted of the amorphous matrix with a very small amount of nanocrystals with a mean diameter of 14 nm. The hardness was almost the same as that of the B.M. (740 HV).

(3) The average tensile strengths of the welded specimen at the welding speeds of 6 m/min and 12 m/min were 771 MPa and 1312 MPa, respectively. The joint efficiencies at 6 m/min and 12 m/min were 33% and 56% of the B.M. (2334 MPa), respectively.

ACKNOWLEDGEMENT

This work was supported by a Grant-in-Aid for Scientific Research on Priority Areas 428 KAKENHI (16039211) and Grant-in-Aid for Cooperative Research Project of Nationwide Joint-Use Research Institutes on Development Basis of Joining Technology for Metallic Glasses and Inorganic Materials from The Ministry of Education, Cultures, Sports, Science and Technology, Japan.

FOOTNOTES

*Graduate Student, Graduate School of Engineering, Osaka University, Suita 565-0871, Japan
Present address: Toyota Motor Corp., Toyota City 471-8571, Japan

REFERENCES

[1]A. Inoue, Bulk Amorphous Alloys, *Preparation and Fundamental Characteristics*, (Trans Tech Publications, 1998).

[2]A. Inoue, "Stabilization of Metallic Supercooled Liquid and Bulk Amorphous Alloys," *Acta Mater.*, **48**, 279–306 (2000).

[3]A. Inoue, "Bulk amorphous and nanocrystalline alloys with high functional properties," *Mater. Sci. Eng. A*, **304–306**, 1–10 (2001).

[4]Y. Kawamura and Y. Ohno, "Spark Welding of $Zr_{55}Al_{10}Ni_5Cu_{30}$ Bulk Metallic Glasses," *Scr. Mater.*, **45**, 127–132 (2001).

[5]T. Shoji, Y. Kawamura, and Y. Ohno, "Joining of $Zr_{41}Be_{23}Ti_{14}Cu_{12}Ni_{10}$ Bulk Metallic Glasses by a Friction Welding Method," *J. Japan Inst. Metals*, **66**, 1055–1062 (2002).

[6]C.H. Wong and C.H. Shek, "Friction Welding of $Zr_{41}Ti_{14}Cu_{12.5}Ni_{10}Be_{22.5}$ Bulk Metallic Glass," *Scr. Mater.*, **49**, 393–397 (2003).

[7]Y. Kawamura and Y. Ohno, "Successful Electron-Beam Welding of Bulk Metallic Glass," *Mater. Trans.*, **42**, 2476–2478 (2001).

[8]Y. Yokoyama, N. Abe, K. Fukaura, T. Shinohara, and A. Inoue, "Electron-Beam Welding of $Zr_{50}Cu_{30}Ni_{10}Al_{10}$ Bulk Glassy Alloys," *Mater. Sci. Eng. A*, **375–377**, 422–426 (2004).

[9]T. Zhang and A. Inoue, "New Bulk Glassy Ni-Based Alloys with High Strength of 3000 MPa," Mater. Trans., **43**, 708–711 (2002).

[10]A. Inoue, W. Zhang, and T. Zhang, "Thermal Stability and Mechanical Strength of Bulk Glassy Ni-Nb-Ti-Zr Alloys," Mater. Trans., **43**, 1952–1956 (2002).

[11]C. Qin, W. Zhang, H. Nakata, H. Kimura, K. Asami, and A. Inoue, "Effect of Tantalum on Corrosion Resistance of Ni-Nb(-Ta)-Ti-Zr Glassy Alloys at High Temperature," Mater. Trans., **46**, 858–862 (2005).

[12]S. Yamaura, H. Kimura, and A. Inoue, "The Properties of Bulk Metallic Glasses Related to Hydrogen," *KINZOKU (Mater. Sci. & Tech.)*, **75**, 48–53 (2005).